Mitochondria Are Linked to Calcium Stores in Striated Muscle by Developmentally Regulated Tethering Structures

Simona Boncompagni,* Ann E. Rossi,† Massimo Micaroni,‡
Galina V. Beznoussenko,‡ Roman S. Polishchuk,‡ Robert T. Dirksen,†§
and Feliciano Protasi*§

*Interuniversity Institute of Myology, Department of Basic and Applied Medical Sciences, CeSI-, Università
degli Studi G. d'Annunzio, I-66013 Chieti, Italy; †Department of Pharmacology and Physiology, University of
Rochester Medical Center, Rochester, NY 14642; and ‡Telethon Electron Microscopy Core Facility, Department
of Cell Biology and Oncology, Consorzio Mario Negri Sud, I-66030 Santa Maria Imbaro, Chieti, Italy

Bi-directional calcium (Ca²⁺) signaling between mitochondria and intracellular stores (endoplasmic/sarcoplasmic reticulum) underlies important cellular functions, including oxidative ATP production. In striated muscle, this coupling is achieved by mitochondria being located adjacent to Ca²⁺ stores (sarcoplasmic reticulum [SR]) and in proximity of release sites (Ca²⁺ release units [CRUs]). However, limited information is available with regard to the mechanisms of mitochondrial-SR coupling. Using electron microscopy and electron tomography, we identified small bridges, or *tethers*, that link the outer mitochondrial membrane to the intracellular Ca²⁺ stores of muscle. This association is sufficiently strong that treatment with hypotonic solution results in stretching of the SR membrane in correspondence of tethers. We also show that the association of mitochondria to the SR is 1) developmentally regulated, 2) involves a progressive shift from a longitudinal clustering at birth to a specific CRU-coupled transversal orientation in adult, and 3) results in a change in the mitochondrial polarization state, as shown by confocal imaging after JC1 staining. Our results suggest that tethers 1) establish and maintain SR–mitochondrial association during postnatal maturation and in adult muscle and 2) likely provide a structural framework for bi-directional signaling between the two organelles in striated muscle.

INTRODUCTION

Calcium ions (Ca²⁺) are versatile second messengers that play a key role in a variety of cellular physiological functions, including gene expression, differentiation, neurotransmitter release, muscle contraction, motility, and communication between cells (Rasmussen *et al.*, 1976; Endo, 2006). In addition, Ca²⁺ ions also provide a mechanism for communication between different subcellular compartments (e.g., endoplasmic/sarcoplasmic reticulum [ER/SR] and mitochondria). A large electrochemical gradient (> -180 mV) provides a substantial driving force for mitochondrial Ca²⁺ entry that occurs through several postulated mechanisms that include 1) a ruthenium red–sensitive uniporter (Gunter and Gunter, 1994), 2) a rapid mode Ca²⁺ transport mecha-

nism (Buntinas *et al.*, 2001), and 3) a mitochondrial ryanodine receptor (Beutner *et al.*, 2001). Entry of Ca²⁺ into the mitochondrial matrix stimulates the respiratory chain, which increases cellular ATP production required to support various cellular functions (e.g., muscle contraction, increased motility, and neurotransmitter release). Specifically, elevations in matrix Ca²⁺ stimulate several mitochondrial dehydrogenases responsible for generating NADH (pyruvate, isocitrate, and 2-oxoglutarate dehydrogenases) and the ATP synthetic capacity of the F_1F_0-ATPase (Territo *et al.*, 2001).

The physiological relevance of mitochondrial Ca²⁺ uptake has been subject to controversy. Indeed, the concentration of Ca²⁺ required for half-maximal mitochondrial Ca²⁺ transport (~ 30 μM; Scarpa and Graziotti, 1973) is considerably higher than that typically achieved during global cytosolic Ca²⁺ transients (~ 1 μM), even in skeletal muscle fibers where large amounts of Ca²⁺ are released from the SR (Crompton *et al.*, 1976; Sembrowich *et al.*, 1985). Nevertheless, direct measurements of mitochondrial Ca²⁺ using targeted Ca²⁺ probes (Rizzuto and Pozzan, 2006; Bolanos *et al.*, 2008) demonstrate that mitochondria sequester Ca²⁺ during cytoplasmic Ca²⁺ oscillations in fibroblasts, endothelial and epithelial cells, neurons, pancreatic acinar cells, and muscle cells, among others (Miyata *et al.*, 1991; Duchen, 1999; Rizzuto and Pozzan, 2006).

The apparent discrepancy between the magnitude of the global Ca²⁺ transient and low-affinity mitochondrial Ca²⁺ transport is reconciled by the concept of local Ca²⁺ microdo-

Abbreviations used: CRUs, calcium release units; EC coupling, excitation-contraction coupling; EDL, extensor digitorum longus; EM, electron microscopy; ET, electron tomography; FDB, flexor digitorum brevis; jSR, junctional SR; MCU, mitochondrial Ca²⁺ uniporter; RyR, ryanodine receptor; SR, sarcoplasmic reticulum; T-tubule (or TT), transverse tubule.

mains: strategic positioning of mitochondria in close proximity to a point source of Ca^{2+} flux (e.g., from the surface membrane and/or ER/SR) is required to drive low-affinity mitochondrial Ca^{2+} uptake mechanisms. Within these privileged signaling microdomains, the Ca^{2+} concentration at the site of influx and release can rise to levels sufficient to activate low-affinity mitochondrial Ca^{2+} transport mechanisms. However, mitochondrial Ca^{2+} uptake needs to be precisely controlled because excessive Ca^{2+} entry will activate the mitochondrial permeability transition pore, resulting in the collapse of the inner mitochondrial membrane potential, release of cytochrome C, and induction of programmed cell death (Duchen, 2000; Joza *et al.*, 2001; Newmeyer and Ferguson-Miller, 2003). Local transient Ca^{2+} fluxes within the microdomain ensure that mitochondria are exposed to a high pulse of Ca^{2+} that is sufficient to activate uptake for only a limited period of time before being terminated as a result of passive diffusion of Ca^{2+} away from the microdomain.

Thus, it has become increasingly critical to determine the spatial disposition of mitochondria within the cell, and importantly, to define their specific positioning and structural interaction to sites of Ca^{2+} flux. Close, intimate structural interactions between ER and mitochondria have been demonstrated in some cell types (Sharma *et al.*, 2000; Csordas *et al.*, 2006; Mannella, 2006). Interestingly, this interorganelle association may be controlled and/or modified under different functional and pathological states, suggesting that the association may exhibit plasticity depending on the developmental or functional state of the cell (Csordas *et al.*, 2006).

Whether or not mitochondrial Ca^{2+} uptake occurs during fast and frequent Ca^{2+} release events in skeletal muscle has been debated for many years. An elegant study (Rudolf *et al.*, 2004) clearly demonstrated significant mitochondrial Ca^{2+} uptake in intact skeletal muscle during both single twitches and tetanic stimulation. Although Ca^{2+} uptake by individual mitochondria is limited, aggregate Ca^{2+} uptake by a sufficiently large number of strategically located mitochondria significantly blunts local and global cytoplasm Ca^{2+} transients under physiological conditions (Rudolf *et al.*, 2004). Similar results were found in single extensor digitorum longus (EDL) and soleus fibers (Shkryl and Shirokova, 2006). Moreover, contractile relaxation is accelerated in mitochondrial-rich skeletal muscle fibers, but not in more glycolytic fibers with fewer active and respiring mitochondria (Gillis, 1997).

In skeletal muscle, available morphological data suggests a close proximity of a large fraction of mitochondria to the SR, in proximity to sites of Ca^{2+} release, or calcium release units (Ogata and Yamasaki, 1987). However, no information is available with regard to either mitochondrial disposition during skeletal muscle development or how this positioning is maintained in adult muscle. Here we describe an "anchoring system" established during skeletal muscle postnatal development that links the outer mitochondrial membrane to the intracellular Ca^{2+} stores.

MATERIALS AND METHODS

Fixation and Embedding of Samples for Electron Microscopy (EM). Mice were killed by cervical dislocation at 0.5, 1, 2, and 4 mo of age in accordance with protocols approved by the University of Rochester School of Medicine and Dentistry University Committee on Animal Resources. Skin was quickly removed from the animal's feet and flexor digitorum brevis (FDB) muscles were fixed in situ with fixative solution (3.5% glutaraldehyde in 0.1 M NaCaCo buffer, pH 7.2) at room temperature. On the other hand, hearts from 3.5-mo-old rats were fixed and embedded as described by Sharma *et al.* (2000) and provided for this study by C. Franzini-Armstrong. Small bundles of fixed muscle fibers or cells from either FDB muscles or hearts were then

postfixed in 2% OsO_4 in the same buffer for 2 h and block-stained in aqueous saturated uranyl acetate. Specimens were rapidly dehydrated in graded ethanol and acetone, infiltrated with Epon 812-acetone (1:1) mixture for 2 h and then embedded in Epon. For T-tubule staining, small fiber bundles were placed overnight in 3.5% glutaraldehyde in 0.1 M sodium cacodylate buffer (pH 7.2, 4°C) containing 75 mM $CaCl_2$. These specimens were then postfixed in a mixture of 2% OsO_4 and 0.8% $K_3Fe(CN)_6$ for 1–2 h followed by a rinse with 0.1 M sodium cacodylate buffer with 75 mM $CaCl_2$ (Sommer and Waugh, 1976; Forbes *et al.*, 1977). Samples were then dehydrated, infiltrated, and embedded as before. Ultrathin sections (~30–40 nm) and semithin sections (100 nm) were cut in Leica Ultracut R (Leica Microsystems, Wien, Austria) using a Diatome diamond knife (Diatome, Biel, Switzerland) and stained in 4% uranyl acetate and lead citrate. All sections were examined with a FP 505 Morgagni Series 268D electron microscope (Philips, Hamburg, Germany) at 60 kV equipped with a Megaview III digital camera and Soft Imaging System (Münster, Germany).

Exposure to Hypotonic Solution before and during Fixation. Small-fiber bundles from either EDL or soleus muscles were carefully separated and immersed in half-strength Ringer's solution for 10 min, fixed in 0.5% glutaraldehyde for 25 min, followed by 25 min in 2% glutaraldehyde, and finally kept in 3.5% glutaraldehyde until the embedding procedure (Nunzi and Franzini-Armstrong, 1980). Samples were then processed as described above.

Quantitation of Mitochondria–CRU Connectivity. Minimum distance between RyR-feet and the outer membrane of the nearest mitochondrion was measured in electron micrographs taken at high magnification (71,000×) using the Soft Imaging System (see Figure 1B, dotted line) and determined from a total of 269 and 297 measurements collected in 2- and 4-mo-old specimens, respectively. To obtain an estimate of the minimum Ca^{2+} diffusional distance between sites of release and mitochondrial Ca^{2+} uptake, a hypothetical diffusion path from RyRs in the jSR to the nearest mitochondrial membrane was drawn in high-resolution images of FDB fibers obtained from 2- and 4-mo-old mice (Figure 1B, dotted line) and measured. Results of these measurements are reported in Table 1, column A.

CRU and mitochondrial density (and their position relative to the sarcomeres) was determined from five to eight micrographs (at 14,000×) of nonoverlapping regions that were randomly collected from longitudinal sections of internal fiber areas. In each EM image, the number of triads and mitochondria was determined, as well as the incidence of mitochondrial positioning with respect to the I and A bands. If an individual mitochondrion extended from one band to the other, it was counted in both. CRUs and mitochondria were marked and counted in each micrograph and the area of the image was determined. The results presented in Table 1 are shown as average (±SD) number of CRUs/100 μm^2 (column B) or mitochondria/100 μm^2 (column C) of cross-sectional area. The percentage of mitochondria located in correspondence with the I band and next to triads at each developmental period was determined and reported Table 1, columns D and E, respectively.

Quantitative analysis of tethers. Average tether length and width of the gap separating SR and mitochondrial membranes were measured from electron micrographs taken at high magnification (71,000×) using the Soft Imaging System (Germany). The distance between the two external leaflets of the SR and mitochondrial membrane was measured both at random points where tethers were not seen (width of junctional gap, n = 92) and in correspondence with tethers (tether length, n = 104). Means (±SD) were determined from individual values by descriptive statistics using Prism v4.0 (GraphPad Software, San Diego, CA; Table 2. The relative frequency of tethers connecting SR to the mitochondrial outer membrane was determined by counting the number of tethers in 100 randomly collected images of mitochondria–CRU pairs at four postnatal time points. Results of these measurements are shown in Figure 6B. The number of tethers per cross-sectional area (Figure 6C) was determined by multiplying for each time point the number of SR–mitochondria pairs in 100 μm^2 (values in Table 1, column E) by the fraction of tethers in 100 mitochondrial–CRU pairs (i.e., values in Figure 6B). The estimation of how frequently one tether occurred together with another tether (or more than one) was determined by counting singles, pairs, and multiple groups of tethers in images of 80 mitochondria–CRU pairs taken at high magnification. Results of this quantitation are reported in Figure 6D.

Electron Tomography and 3D Reconstructions. The analysis of samples by electron tomography was performed on 250-nm-thick sections, as described previously (Koster *et al.*, 1997; Ladinsky *et al.*, 1999). Briefly, 5- or 10-nm gold particles were placed on both surfaces of the plastic sections (prepared as described above). Tilt series were collected automatically at 120 kV accelerating voltage and at 1° increments over an angular range of −65° to +65° on FEI Tecnai-12 microscope (FEI, Eindhoven, Netherlands) using Xplore3D software (FEI). Digital images from the regions of interest were captured at 43,000× magnification in each tilt position (131 in total) using a Megaview III CCD camera and exported to either PC Power Station equipped with Inspect 3D software (FEI) or a Silicon Graphics computer (Sunnyvale, CA) running the IMOD software (IMOD program package, University of Denver, Denver, CO). These digital images were then used to generate initial 3D reconstruc-

Table 1. Quantitative analysis of mitochondria, CRUs and maturation of SR-mitochondrial connectivity in FDB fibers (0.5 – 4 months of age)

Age	A — Nearest distance between RyRs and mitochondrial outer membrane (nm)[b]	B[a] — No. of CRUs/100 μm^2 [c]	C[a] — No. of mitochondria/100 μm^2 [c]	D[a] — % of mitochondria at the I band[d]	E[a] — No. of mito-CRU pairs/100 μm^2 [e]
0.5 mo	—[f]	21 ± 5	27 ± 7	52	7 ± 2 (26)
1 mo	—	43 ± 9	32 ± 9	76	13 ± 3 (41)
2 mo	131 ± 50 (269)	69 ± 12	59 ± 13	88	38 ± 5 (64)
4 mo	128 ± 38 (297)	88 ± 25	75 ± 24	99	60 ± 9 (80)
Average $\pm$ SD	130 ± 45 (566)				

(Column A) The distance between sites of Ca^{2+} release and the nearest outer mitochondrial membrane was measured at 2 and 4 months of age by drawing a curved line as shown in Figure 1D. (Columns B and C) The number of CRUs and mitochondria per unit area increases progressively from 2 weeks to 4 months of age. Data are given as mean ($\pm$ SD) number of CRUs and mitochondria per 100 μm^2. (Columns D and E) Percentages of mitochondria located at the I band and number next to a CRUs. In Column E, the percentage of mitochondria coupled to CRUs is reported in parentheses. Both values increase progressively with age, indicating that in addition to an increase in number of mitochondria and triads, positioning of mitochondria to the I band and their association with triads also increase steadily during postnatal development.

[a] Sample size is 80 pictures/10 fibers/2 animals per time point.
[b] Values are the mean$\pm$ SD, with the number of measurements in parentheses.
[c] Values are mean$\pm$ SD.
[d] Values are the percentage of the total.
[e] Values are the mean$\pm$ SD of the number of measurements, with the percentage of the total number of mitochondria paired to CRUs.
[f] —, not measured.

tions (tomograms) on the basis of ART and SIRT algorithms. Tomogram resolution was calculated by Xplore3D software (FEI) on the basis of resolution obtained from tilt images and ranged from 3.8 to 4.9 nm. The accuracy of the resolution was confirmed via analysis of neighboring 5-nm gold particles (located at the section surface), which were easily resolvable from each other. Tomograms were then used to construct surface models (shown in Figure 2, D–F, and in Supplemental Figure S2) by coloring the outlines of membranes (SR, T-tubule, and mitochondrion) and electron densities (RyR-feet and tethers). All together, 12 tomograms were obtained.

Confocal Analysis of Mitochondrial Localization during Development. Single acutely dissociated FDB muscle fibers were isolated from young (0.5 and 1 mo old) and adult (2 and 4 mo old) C57B/6J mice as described previously (Lueck *et al.,* 2007). To assess mitochondrial position with respect to T-tubule localization, fibers were loaded simultaneously with 100 nM MitoTracker green (Molecular Probes/Invitrogen, Eugene, OR) and 5 μM di-8-ANEPPS (Molecular Probes/Invitrogen). Di-8-ANEPPS and MitoTracker green fluorophores were sequentially excited using 543 nm (8$\times$ attenuation, 605/75-nm emission) and 488 nm (4$\times$ attenuation, 515/30-nm emission) lasers, respectively. All images (512 $\times$ 512, 0.08 μm/pixel) were acquired and averaged (n = 4) using a Nikon Eclipse C1 Plus Confocal microscope (30 μm pinhole) equipped with a SuperFluor 40$\times$ 1.3 NA oil objective (Nikon Instruments,

Melville, NY). To assess relative changes in mitochondrial membrane potential during development, young and adult FDB fibers were loaded with 1.5 μM JC-1 (Molecular Probes/Invitrogen) in Ringer's solution for 20 min at 37°C. With the focal plane positioned at the center of the fiber, JC-1 was excited using a 488-nm laser (8$\times$ attenuation, 515- and 605-nm emission) to produce an average 47.7 $\times$ 47.7-μm image (n = 4). A composite average ratio (red/green) image of JC-1 aggregate (red) and JC-1 monomer (green) fluorescence was subsequently created offline. A 20-μm line along the longitudinal axis of the fiber was drawn to generate a mean XY ratio profile, with X values representing fiber width and Y values representing the longitudinally averaged fluorescence ratio. Because each line length varied with fiber width, all X values were normalized to the longest X value, yielding a percent of the fiber width for each profile. The ratio values were binned and averaged every 2% according to their corresponding X-coordinates. To enable comparison between different fibers, images were recorded using identical laser power, photomultiplier sensitivity and were processed using identical values for contrast and brightness. Images were processed and analyzed using NIH ImageJ (http://rsb.info.nih.gov/ij/) and AutoQuant AutoDeblur and AutoVisualize (Media Cybernetics, Silver Spring, MD) software packages.

Mitochondrial Movement in HEK293 Cells and Adult FDB Fibers. Time-lapse confocal microscopy was used to assess relative mitochondrial movement in HEK293 cells and adult FDB fibers expressing a mitochondria-targeted enhanced yellow fluorescent protein (EYFP-Mito, BD Biosciences, San Jose, CA). HEK293 cells grown on glass coverslips were transfected using FuGene 6 Transfection Reagent (Roche, Indianapolis, IN) according to manufacturer's recommendations. EYFP-Mito was expressed in adult FDB fibers using an electroporation approach described previously (DiFranco *et al.,* 2006). Briefly, wild-type C57B/6J mice were anesthetized by intraperitoneal injection of 100 mg/kg ketamine, 10 mg/kg xylazine, and 3 mg/kg acepromazine. FDB muscle was pretreated by intramuscular injection of bovine hyaluronidase (15 μl, 0.4 U/μl; Sigma-Aldrich, St. Louis, MO). One hour later, 80 μg of pEYFP-Mito (BD Biosciences) in a total volume of 20 μl, 71 mM NaCl was injected using a 30-gauge needle. FDB muscle was then electroporated using electrodes placed perpendicular to the long axis of the muscle. Electroporation parameters were 100 V/cm, 20 ms duration, and 20 pulses delivered at 1 Hz. One week later, single muscle fibers from electroporated FDB muscles were isolated by enzymatic dissociation as described above. EYFP-Mito was excited using a 488 nm (64$\times$ attenuation, 515/30 nm emission) laser. Time series (60 total frames, 3 min) were acquired using a Nikon Eclipse C1 Plus Confocal microscope (30 μm pinhole) equipped with a SuperFluor 40$\times$ 1.3 NA oil objective (Nikon Instruments). Each acquired image was 592 $\times$ 592 pixels (0.08 μm/pixel), and the average of two consecutive images. Image sequence movies (frames/s) were created offline using AutoQuant AutoDeblur & AutoVisualize (Media Cybernetics) and NIH ImageJ software packages.

Table 2. Tether length (nm) during postnatal development (0.5–4 months of age)

Age/gender	Tether length
0.5 mo/male	9.1 ± 2.9 (22)
1 mo/male	9.3 ± 2.1 (17)
2 mo/male	9.9 ± 1.5 (22)
4 mo/male	11.7 ± 3.2 (42)
Average$\pm$ SD	10.4 ± 2.8 (104)

Tether length was measured at all four postnatal developmental time points (0.5–4 months). Tethers typically appear as short thin strands, a few (3–4) nm in diameter, with an average length (10.4 $\pm$ 2.8 nm) that does not change significantly during postnatal development.

Values are mean$\pm$ SD, with the number of measurements in parentheses.
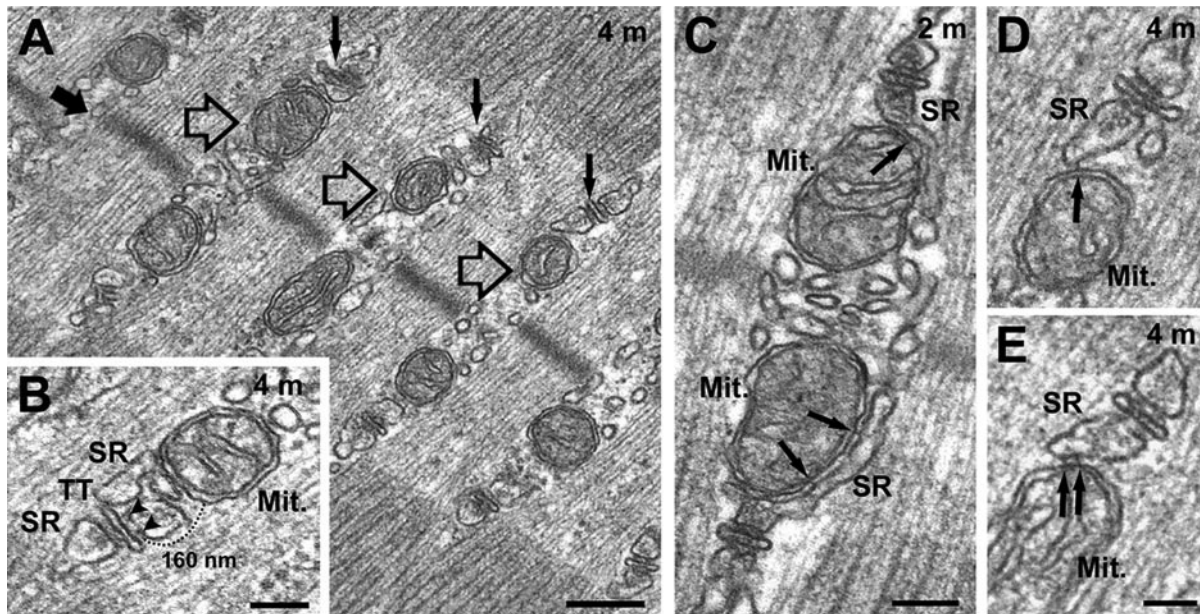
Figure 1. Mitochondria and CRUs are closely apposed to each other and connected by small electron dense strands, or tethers. (A) In adult muscle fibers, triads (small black arrows) are located in proximity of the sarcomere A-I band junction. Mitochondria (open arrows) are positioned adjacent to the triad, on the side opposing the Z-line (large black arrow). (B) Mitochondria associated with the SR terminal cisternae on the side opposite to that of the Ca^{2+} release channels, or RyRs (arrowheads). Dashed line shows the shortest distance between release sites (RyR-feet) and the outer mitochondrial membrane (see Table 1, column A for quantification). (C–E) Under higher magnification, small electron-dense strands (black arrows) appear to tether, or bridge, individual mitochondria (Mit.) to the triad. This structural linkage occurs specifically between the mitochondrial outer membrane and the SR terminal cisterna, generally on the side opposite to that facing the T-tubule (D and E), but also between mitochondria and the lateral sacks and tubules of the SR that surround the mitochondrion (C). Interestingly, these structures are often found in pairs (E; see also Figure 6D for quantitation). Bars, (A) 0.25 μm; (B and C) 0.1 μm; (D and E) 0.05 μm.

Statistical Analysis. Data are given as mean $\pm$ SD in Tables 1 and 2. Data in Supplemental Figure S3B are reported as mean $\pm$ SE. Differences were considered statistically significant at $p < 0.05$.

RESULTS

Mitochondria in Adult FDB fibers Are Preferentially Localized Adjacent to the CRU. Previous studies indicate a close proximity between mitochondria and SR in both skeletal and cardiac muscle fibers (Ogata and Yamasaki, 1985; Sharma *et al.,* 2000). Differences have also been shown between mitochondrial disposition in fast versus slow twitch skeletal fibers. In fast twitch fibers, mitochondria are found mostly in correspondence of the I band, whereas in slow twitch fibers mitochondria are also found in longitudinal clusters between myofibrils and under the sarcolemma (Ogata and Yamasaki, 1985). In fast twitch FDB fibers from adult mice (2–4 mo old) subsarcolemmal mitochondria are rarely found and most mitochondria are located within the space between the sarcomere A-I band junction and the Z-line (Figure 1A). Mitochondria are usually closely apposed to the SR, adjacent to CRUs or triads (Figure 1B). Interestingly, association of mitochondria with the triad occurs exclusively on the side of SR terminal cisterna that faces the Z-line of the sarcomere, positioning mitochondria within the I band zone.

CRU-associated mitochondria may be round or slightly elongated, and they either partially or fully encircle the myofibrils at two positions on either side of the Z-line. The triads, in turn, are located immediately adjacent to the mitochondria, such that one of the two SR lateral sacs, the one nearest the Z-line, is adjacent to the outer membrane of the associated mitochondrion (Figure 1B). Triads and mitochondria are elongated in sections that cut along the long axis of the CRU and, as a result, the two organelles run parallel to each other over relatively long distances (>1 μM), constituting a structural mitochondrion-triad unit (see Supplemental Figure S1).

Given the potential functional impact of positioning mitochondria adjacent to site of Ca^{2+} release (see *Introduction*), we measured the distance between ryanodine receptors (RyRs), the SR Ca^{2+} release channels, and the closest associated mitochondrion. RyRs, seen as "feet" in thin sections, are clustered in two rows of ordered arrays in mature junctions. These ordered arrays of RyRs are located on the surface of the junctional SR (jSR) cisterna that faces away from the mitochondrion and toward the T-tubule (Figure 1B, small arrowheads). To obtain an estimate of the minimum Ca^{2+} diffusional distance between sites of release and mitochondrial Ca^{2+} uptake, a hypothetical diffusion path from RyRs in the jSR to the nearest mitochondrial membrane was drawn in high-resolution images of FDB fibers obtained from 2- and 4-mo-old mice (Figure 1B, dotted line) and measured. The minimum distance between the RyRs and the nearest mitochondrial membrane was 130 ± 45 nm (Table 1, column A).

CRUs and Mitochondria Are Connected by Small Electron-Dense Tethers. To characterize the three-dimensional (3D) interface between the mitochondrial and SR membranes in greater detail, we combined the powers of transmission EM and electron tomography (ET). Under higher magnification, we identified short bridges, termed *tethers*, which connect the outer mitochondrial membrane to sacs of the adjacent SR (Figure 1, C–E). Tethers typically appear as short, thin strands, a few (three or four) nanometers in diameter, with a quite uniform length (10.4 ± 2.8 nm, Table 2). In thin
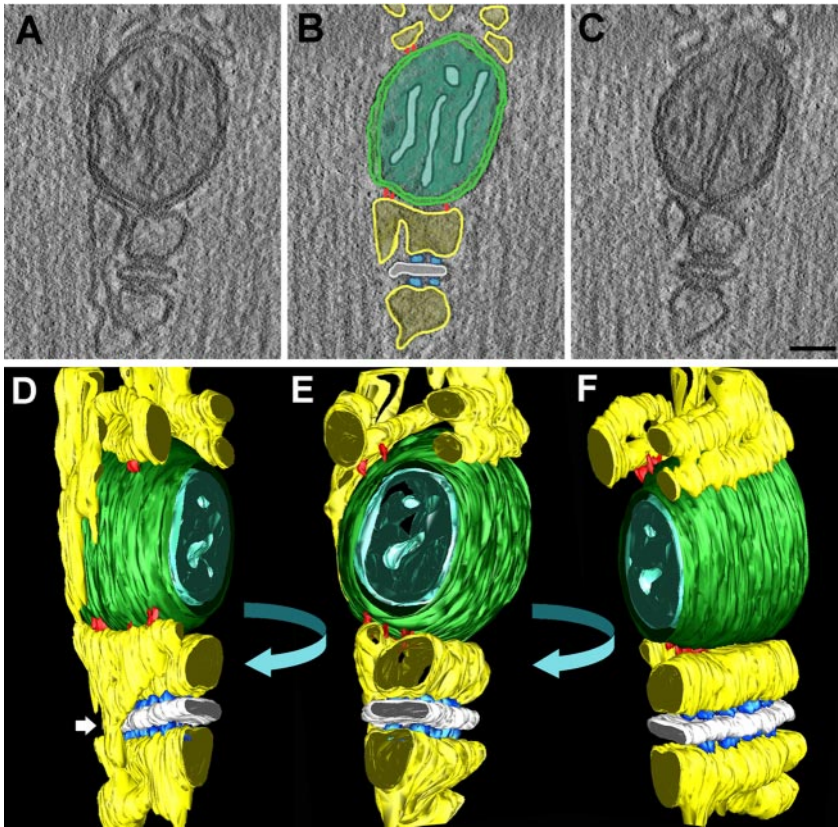
Figure 2. Tomography and 3D reconstruction of a mitochondrion–CRU unit. (A–C) Three representative images (out of 131 total) from one tomography are shown (see also Supplemental Movie 1). (D–F). Three representative orientations are shown for the 3D reconstruction of the mitochondria–CRU unit shown in A–C (see also Supplemental Movie S2, A–E). Two major details are apparent from these reconstructions: 1) tethers are sometimes found in clusters of 3–5 elements; and 2) free SR elements often connect two jSR cisternae from opposite sides of the T-tubules (white arrow in D). yellow, SR; white, T-tubule; outer mitochondrial membrane green, outer mitochondrial; cyan, inner mitochondrial membrane; azure, RyR-feet; red, tethers. Bar, (A–C) 0.05 μm.

sections, tethers are usually visualized as either a singlet or doublets (Figure 1, C–E), but rarely in groups of three or more (see Figure 6D for more detail). Although tethers are most frequently detected at the contact between the mitochondrion and the terminal cisterna, they are also observed in lateral sacks and tubules of the SR where the longitudinal (free) SR abuts the sides of the mitochondrion (Figure 1C). ET was used to reconstruct a whole triad-mitochondrion assembly and to determine the 3D architecture of the interface between the two closely associated organelles (Figure 2; see also Supplemental Figure S2 and Supplemental Movies S1 and S2, A–E). Two major details result from these reconstructions. First, tethers are sometimes found in clusters of three to five elements, a detail that is missed in 2D images from thin section (Figure 1, C–E). Second, free SR elements often connect two jSR cisternae from opposite sides of the T-tubules, thus creating a longitudinal continuity in the SR lumen (Figure 2D, white arrow).

Tethers Provide a Mechanical Link within the Triad-Mitochondrion Assembly. If tethers provide a mechanism for holding SR and mitochondria together, then defined, constant distance between the two organelles would be expected when the two compartments are linked together with tethers. To determine if this is the case, we measured the average width of the gap separating adjacent membranes of the two organelles in correspondence of tethers (tether length; see Table 2) and in regions where tethers were not seen. Consistent with the hypothesized tether-coupling model, the average distance between the two organelles is significantly smaller and less variable when tethers are observed (10.4 ± 2.8 nm, n = 104), compared with when they are not (14.4 ± 4.9 nm, n = 92; p < 0.001). These findings are

consistent with tethers anchoring the mitochondrion to the SR. They also provide evidence for a unique and structurally homogeneous tethering element.

One other experiment was used to further define whether tethers provide a mechanical link between the SR and the mitochondrial outer membrane. We treated muscle fiber bundles with a hypotonic (50% physiological osmolarity) solution before and during fixation (Figure 3). This procedure was expected to induce membrane swelling of attached organelles and thus create significant mechanical stress on their junctions. After hypotonic treatment, the jSR exhibits compact and electron-dense areas (those containing calsequestrin) alternated with areas of significant swelling (Figure 3A). All cytoplasmic volumes are enlarged, creating apparently empty spaces between the SR and myofibrils (not shown) and importantly, also increasing separation between the SR and mitochondria (cf. Figure 3A and Supplemental Figure S1B). In spite of an overall increase in SR–mitochondrial separation, electron dense tethers are still observed at discrete regions of contact between the SR and the associated mitochondrion (Figure 3, small arrows). These results indicate that tethers provide a structural anchor between the SR and associated mitochondrion that maintains a narrowly defined intercompartment distance, even as the two organelles are pulled apart by mechanical stress.

Mitochondrion-CRU Colocalization Is Increased during Postnatal Development. We determined mitochondrial localization in single, isolated FDB muscle fibers at four different stages of postnatal development (0.5, 1, 2, and 4 mo) using confocal microscopy. In each case, fibers were co-loaded with di-8-ANEPPS to stain surface and T-tubule membranes and MitoTracker Green, a mitochondrial-selec-
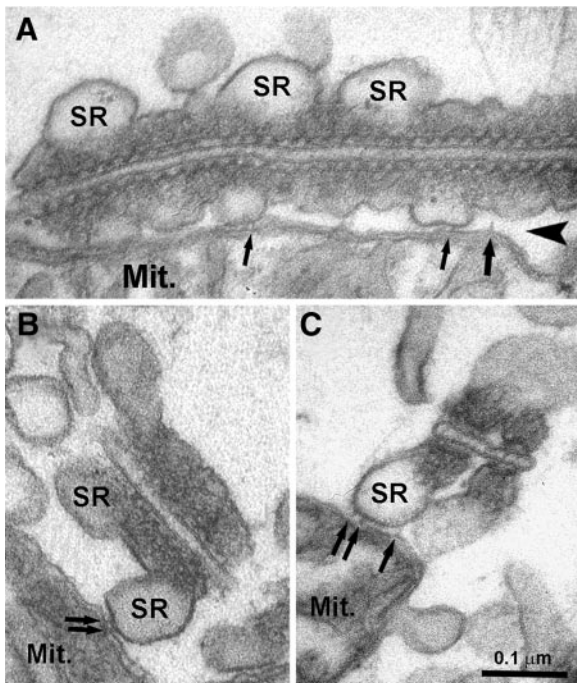
Figure 3. SR–mitochondrial tethers remain after SR swelling induced by hypotonic shock. (A) Exposure to hypotonic solution results in SR and mitochondrial swelling and in increase of intermembrane distances between the SR and mitochondria (arrowhead). However, SR–mitochondrial physical association is sufficiently strong to withstand swelling produced by hypotonic shock (small back arrows). Occasionally, putative disrupted or unattached tethers are observed after hypotonic shock (larger arrow). (B and C) After hypotonic shock, SR vesicles appear to stretch exactly in correspondence with structures tethered to the adjacent mitochondrion (arrows). Bar, 0.1 μm.

tive fluorescent probe. Mitochondria in FDB fibers from 0.5-mo-old mice are arranged primarily in subsarcolemmal and longitudinal clusters within the myofibrillar space (Figure 4, A and B, green signal). On the other hand, a primitive T-tubule system has begun to develop in 0.5-mo-old fibers, even if not completely (see next section), as evidenced by

fibers exhibiting double rows of transverse di-8-ANEPPS staining, consistent with the known location of the T-tubule network at the A-I junction in mammalian muscle (Figure 4, A and B, red signal). Strong colocalization of MitoTracker Green and di-8-ANEPPS signals along the sarcolemma (Figure 4, A and B, yellow areas) is indicative of a subsarcolemmal population of mitochondria in 0.5-mo-old FDB fibers. The absence of significant transverse MitoTracker Green and di-8-ANEPPS colocalization suggests that mitochondria are not well localized to the triad junction at this stage of postnatal development.

Subsarcolemmal and longitudinal clusters of mitochondrial fluorescence are not typically observed in adult FDB fibers (Figure 4, C and D, 4 mo). Instead, mitochondria create a strong pattern of MitoTracker Green fluorescence between double rows of transverse di-8-ANEPPS fluorescence. This pattern of alternating rows of MitoTracker Green and di-8-ANEPPS fluorescence with a periodicity of ~2 μM is consistent with the location of mitochondria on either side of the Z-line in adult muscle (Figure 1A).

Progressive positioning of mitochondria to the I band throughout postnatal skeletal muscle development is also observed in FDB fibers stained with the mitochondrial membrane potential indicator, JC-1 (Supplemental Figure S3). Because JC-1 is a potentiometric mitochondrial probe, it enables a relative comparison of mitochondrial membrane potential across each of the developmental time points studied, in addition to its use as an independent confirmation of mitochondrial localization. Specifically, monomers of JC-1 emit green fluorescence and predominate in more depolarized mitochondria, whereas JC-1 aggregates emit red fluorescence and accumulate in mitochondria exhibiting a very negative membrane potential. In both young and adult muscle fibers, puncta of red JC-1 fluorescence were clearly visible, though young fibers exhibited more puncta than adult fibers, and red JC-1 fluorescence was typically more concentrated adjacent to the sarcolemma (Supplemental Figure S3A, left). We also found that the average ratio of JC-1 aggregate (red) to JC-1 monomer (green) fluorescence is significantly ($p < 0.001$) greater in FDB fibers isolated from 0.5- and 1-mo-old mice (1.21 ± 0.02 and 1.58 ± 0.01 at 50% fiber width, respectively) compared with that observed for fibers from 2- and 4-mo-old mice (0.82 ± 0.01 and 0.74 ± 0.01 at 50% fiber width, respectively; Supplemental Figure S3B).
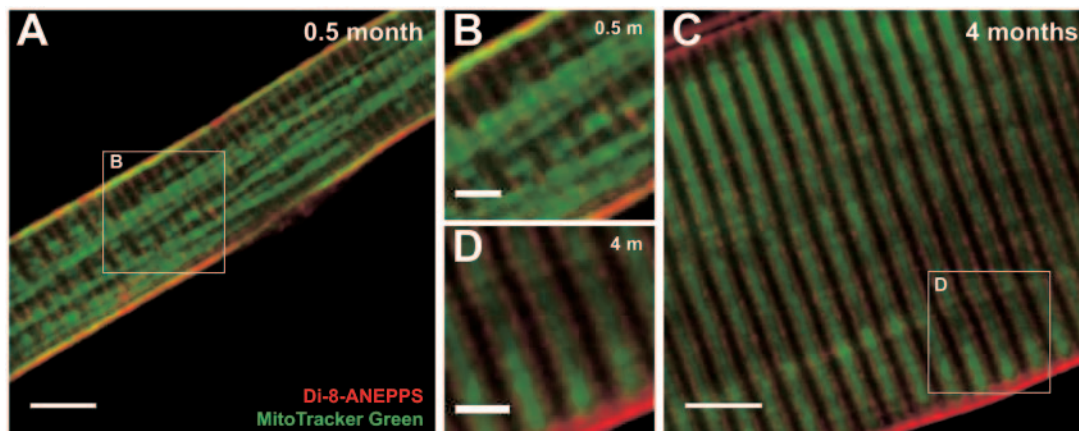

Figure 4. Mitochondrial triad positioning increases during postnatal development. Confocal images of representative FDB fibers obtained from 0.5- (A and B) and 4-mo-old (C and D) mice stained for surface and T-tubule membranes (red, 10 μM di-8-ANEPPS) and mitochondria (green, 100 nM MitoTracker Green). (B and D) Higher magnification images of the boxed regions shown in A and B. A 2D, blind deconvolution was applied to each image for display purposes. Bars, (A and C) 5 μm; (B and D) 2 μm.
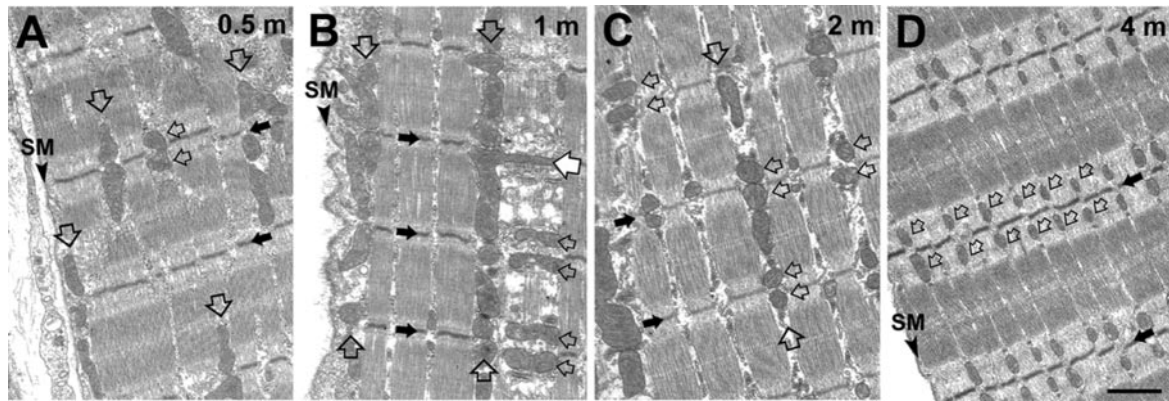
Figure 5. EM analysis of increased mitochondrial triad positioning during development. (A) Two weeks after birth, mitochondria are fewer and typically clustered in small groups and/or longitudinally oriented in rows (open arrows) either under the surface membrane (SM, arrowhead) or between the myofibrils. (B) Although rows and clusters of mitochondria under the SM and between the myofibrils (open arrows) are still frequent 1 mo after birth, a higher percentage of mitochondria are targeted to the I band. During this transition, occasional images show a longitudinal mitochondrion with a long transverse extension (solid white arrow). (C and D) Two to 4 mo after birth, the number of mitochondria per unit area is significantly increased and mitochondria are largely positioned at the I band, on both sides of the Z-line (black arrows). Bar, (A–D) 1 μm.

The decrease in JC-1 emission ratio throughout postnatal development likely reflects a global change in mitochondrial polarization in addition to a decrease in the number of hyperpolarized mitochondria.

Mitochondrial Positioning Next to CRUs Is Stabilized by Progressive "Tethering" during Postnatal Development. Postnatal maturation of muscle fibers (birth to ~1 mo in mice) involves an increase in myofibrillar mass, a gradual reduction intermyofibrillar space, and a dramatic change in both T-tubular development (see Supplemental Figure S4) and mitochondrial localization (Figure 4). Our EM analysis reveals that mitochondria are scarce early in development (0.5 mo), primarily being clustered in small groups located in longitudinal rows that run along the I-A bands and immediately under the sarcolemma (Figure 5A). Also, mitochondrial shape and diameter is more variable early in postnatal development, whereas they are narrower, more regularly shaped, and positioned primarily next to CRUs in fully mature fibers (Figure 5D). The transition between these two arrangements is gradual between 0.5 and 2 mo (Figure 5, A and C) and involves 1) a separation of mitochondria from longitudinal clusters, 2) an elongation in the transverse orientation with a retraction of longitudinal branches, 3) a specific localization at the I band in proximity to the triad, and 4) a change from a variable shape to one that is more consistently narrow and elongated. During this transition, occasional images show a longitudinal mitochondrion with a long transverse extension (Figure 5B, solid white arrow), presumably reflecting repositioning into a transverse orientation.

The progressive shift of mitochondria from longitudinal rows to transverse orientation parallels the progressive postnatal maturation of the sarcotubular system. Longitudinal sections of FDB fibers embedded with a procedure that stains the T-tubule network with a dark precipitate reveal that T-tubules are still fairly disordered at 0.5 mo, exhibiting a considerable amount of longitudinal components (see Supplemental Figure S4, A and B). By 4 mo, the T-tubule network exhibits a more regular transverse orientation and is almost exclusively located at the boundaries of the A band (see Supplemental Figure S4, C and D). Quantification of mitochondrial location during development supports this transition as the number of both CRUs and mitochondria increase progressively from 0.5 to 4 mo of age (Table 1, columns B and C), indicating that skeletal muscle is not fully mature even at 2 mo of age. In addition to the observed increase in triad and mitochondrial number with development, a parallel change in mitochondrial position from random to specific localization next to the triad was also observed. Specifically, the frequency of mitochondria localized to either the I or A band is approximately equal at 2 wk after birth, whereas I band-restricted localization increases sharply up to 99% at 4 mo (Table 1, column D). As a consequence, the number of mitochondrion–CRU units also increases proportionally (Table 1, column E).

The number of mitochondrion–CRU assemblies increases substantially during postnatal development as a result of a progressive increase in both 1) the number of CRUs and mitochondria (Table 1, columns B and C) and 2) the positioning of mitochondria to the I band (Table 1, column D). We hypothesized that tethers play a key role in positioning and maintaining mitochondria next to CRUs (see *Tethers Provide a Mechanical Link…* above). Using EM, we found that tethers are observed at all postnatal developmental stages (Figure 6A), but are more difficult to detect at early stages. We calculated the number of tethers in 100 mitochondrion–CRU assemblies for each developmental time point (0.5, 1, 2, and 4 mo). This analysis revealed that a substantial increase in tether frequency occurs between 0.5 and 1 mo of age and then subsequently levels off (Figure 6B). However, because the number of both mitochondria and CRUs increase during the first 4 mo of postnatal development (Table 1, columns B and C), we calculated the number of tethers per 100 μm^2 of cross-sectional area by multiplying for each developmental time point values in Figure 6B by the average number of mitochondrial–CRU pairs per 100 μm^2 (values in Table 1, column E) for each developmental time point. The result indicates a steady increase in tether number/100 μm^2 between 0.5 and 4 mo of age (Figure 6C) that reflects a combination of increased mitochondrial density (Table 1, column C), progressive targeting of mitochondria to the I band (Table 1, column D), and increased contact with the SR (Table 1, column E). Although these measurements were generated from 2D sections, the results are proportional to the number of tethers per fiber volume.
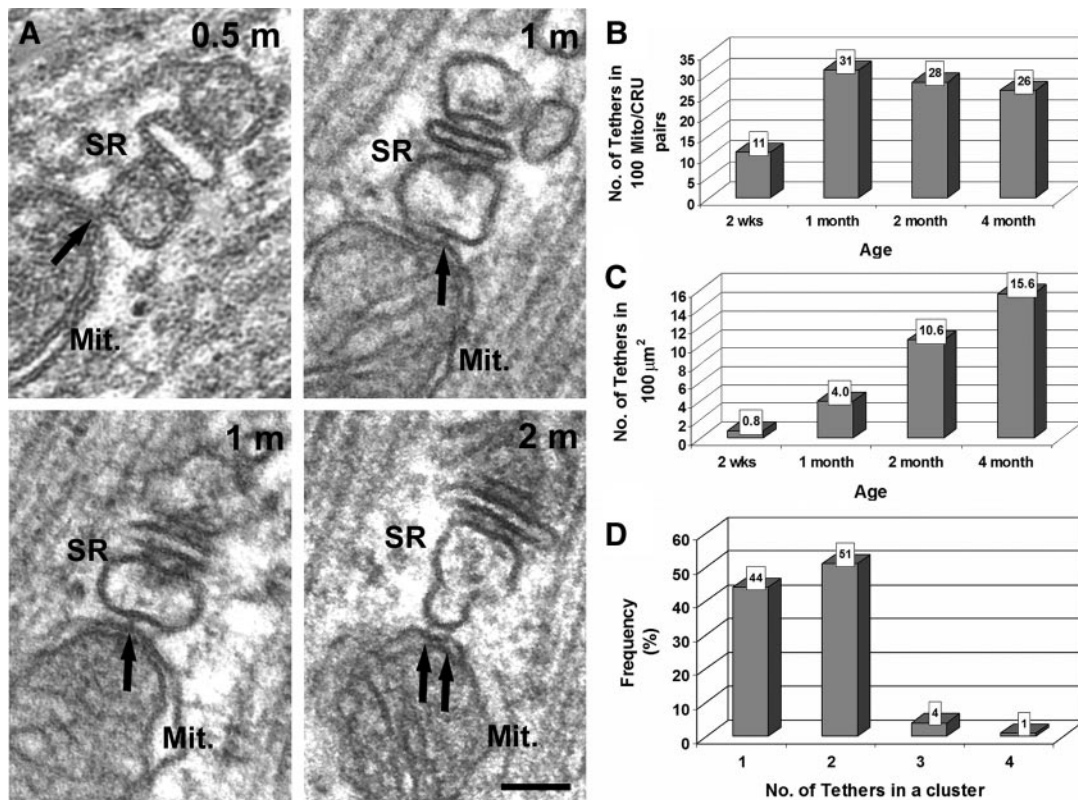
Figure 6. Tethers frequency increases with age and primarily occurs alone or as pairs. (A) Tethers were also found in FDB fibers at all postnatal stages of development. (B) The number of tethers observed in 100 mitochondria–CRU assemblies illustrates that specific positioning of mitochondria to the triad increases markedly during the first month of age and then levels off. (C). The calculated number of tethers (see *Materials and Methods*) per cross-sectional area increases progressively from 2 wk to 4 mo of age. (D) Tethers most frequently occur either alone or in pairs (1 and 2 on the X axis; see also Figure 5 for representative images). Occasionally, three or four tethers close to each other are also observed (3 and 4 on the X axis): indeed, 3D tomographic reconstructions indicate that clusters of multiple tethers are present (see Figure 2 and Supplemental Figure S2 for more detail). Bar, (A) 0.05 μm.

DISCUSSION

The positioning of mitochondria in fast twitch fibers from adult mammalian skeletal muscle is dictated by the repetitive, highly ordered, and tightly packed nature of the myoplasmic space. In adult fast-twitch muscle, mitochondria are targeted to a narrow space within the I band, between the Z-line and the triad (Ogata and Yamasaki, 1987). In this position, mitochondria exhibit a long thin shape that engulfs the myofibrils as a ring. Unlike other cell types in which mitochondria are dynamic organelles that exhibit a significant degree of motility within the cytoplasm (Bereiter-Hahn and Voth, 1994), triad-targeted mitochondria in adult skeletal muscle are remarkably stable and immotile (see Supplemental Movies S3 and S4). Because CRU–mitochondrion Ca^{2+} cross-talk in skeletal muscle operates via local signaling microdomains (Shkryl and Shirokova, 2006), this "privileged" signaling could best be ensured by restricting mitochondria to a location immediately adjacent to sites of Ca^{2+} release by a strong structural anchoring mechanism.

Here we describe the formation of a highly stable association between mitochondria and SR that results in a close proximity between energy-producing organelles and sites of Ca^{2+} release, or CRUs (Figure 1). Multiple 10-nm long electron-dense tethers observed in EM images and ET reconstructions appear to provide an *anchoring structure* that stabilizes the mitochondrion–CRU assembly in skeletal muscle. This mitochondrial anchoring mechanism is likely to be applicable to a wide vari-

ety of excitable and nonexcitable cells. Indeed, structures involved in a similar linkage have been observed between specific ER elements and mitochondria in liver cells (Mannella *et al.*, 1998; Csordas *et al.*, 2006), and similar results are also observed between mitochondria and the SR in adult ventricular cardiomyocytes (Figure 7). Tethers in cardiac cells appear similar to those observed in skeletal fibers and also occur between mitochondria and the SR in proximity to RyRs and sites of Ca^{2+} release (see Figure 7 for more detail).

As mitochondrial Ca^{2+} uptake during transient elevations in cytoplasmic Ca^{2+} requires communication through spatially confined, local signaling microdomains, the intimate mitochondrion–CRU assembly described here provides the structural framework required for local mitochondrial Ca^{2+} uptake observed during SR Ca^{2+} release in adult skeletal muscle (Gillis, 1997; Rizzuto *et al.*, 1998; Shkryl and Shirokova, 2006). We found that tethers bridge SR to mitochondria on the side opposite to the location of RyR-feet. As Ca^{2+} release channels, do not directly face the mitochondria, Ca^{2+} released from the SR must diffuse out of the triad junction and around the SR cisternae before reaching the adjacent mitochondrion (see Figure 1B).

Our findings suggest that SR–mitochondrial tethers in striated muscle may play an important role in trapping and maintaining the mitochondrion at the triad once the two organelles come in close proximity to one another. This idea is indirectly supported by a parallel increase during postna-
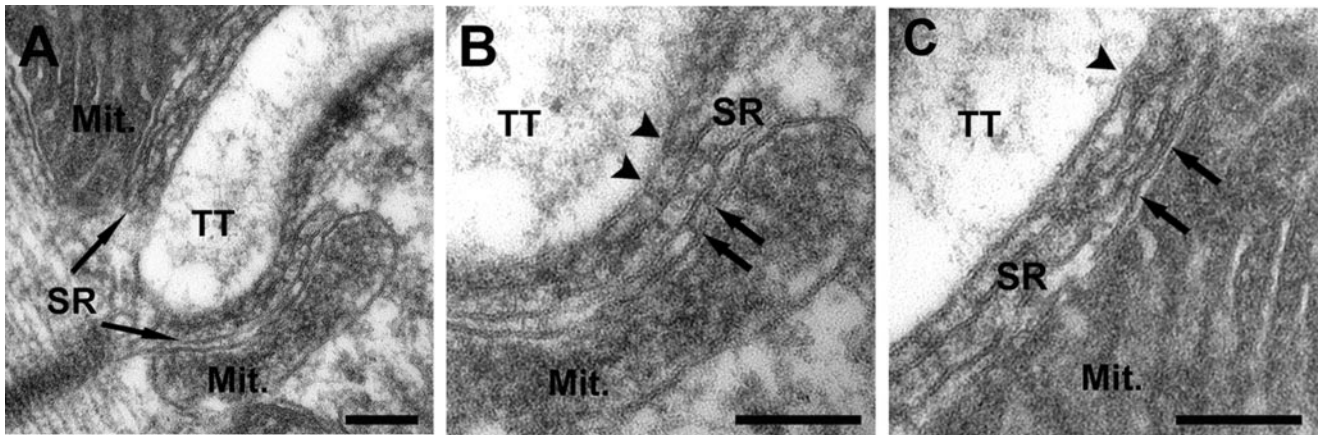
Figure 7. SR–mitochondrial tethers are also observed in cardiomyocytes. (A) In cardiac muscle, T-tubule (TT) diameter is usually quite large, whereas the junctional SR is narrow, flat, and often squeezed between the TT and mitochondrial (Mit.) membranes. (B and C) Electron-dense tethers, similar to those observed in skeletal muscle (see Figures 1 and 6), are also observed in cardiac muscle between mitochondria and SR (small arrows). Also similar to skeletal muscle, mitochondria are positioned on the SR site opposite to that bearing RyR-feet (arrowheads). Bars, (A–C) 0.1 μm.

tal development in the number of triads and mitochondria, the positioning of mitochondria to parajunctional regions (Table 1), and tether number per cross-sectional area (Figure 6C). A proposed scenario underlying the observed changes in mitochondrial disposition during skeletal muscle postnatal development is depicted in Figure 8. Early in muscle development, mitochondria move more freely in the myoplasm because of limited space constraints (Figure 8A). Consistent with this, intermyofibrillar space is greater early in development because myofibrils are not as tightly packed together. Given this greater space and freedom of mobility, mitochondria exhibit more variability in shape and are longitudinally oriented between the myofibrils. As part of this freedom of movement, mitochondria are able to penetrate in the narrower circumferential locations around the myofibrils, predominantly in the I band, where there is increased space availability compared with the more tightly packed A band region (Figure 8B). By mass-action, preferential concentration of triads and mitochondria within the I band region would provide a means by which concurrent expression of tethering machinery could coordinate anchoring of the two organelles in a fixed position (Figure 8C). This scenario is supported by the fact that mitochondrion–CRU assembly and tether frequency are greatly increased during the first month of postnatal development. In addition, an increase in triad frequency occurs in parallel with the increase in the number of mitochondria at the I band. The triads, in turn, are permanently anchored to the myofibrils (Nunzi and Franzini-Armstrong, 1980), presumably via obscurin (Bagnato *et al.,* 2003). Interestingly, the maturation of the T-tubule network follows a similar postnatal time course and pattern. Specifically, T-tubules initially assume a longitudinal orientation between the myofibrils and then, through an association with the triad, later establish the classic transverse orientation observed in adult skeletal muscle (Takekura *et al.,* 2001). Thus, a series of structural linkage proteins orchestrate a highly coordinated and ordered arrangement of the mitochondrion–CRU assembly and their relationship with myofibrils: obscurin docks the terminal SR to the myofibrils (Bagnato *et al.,* 2003), junctophilin connects the terminal SR to the T-tubule (Takeshima *et al.,* 2000; Ito *et al.,* 2001), and electron-dense tethers anchor the mitochondrial outer membrane to the SR (this article).

Our measurements demonstrate that both tether frequency and mitochondrion–CRU assembly incidence increase dramatically during postnatal development. This bicompartment assembly may be functionally relevant as the lack of mitochondrial targeting adjacent to sites of Ca^{2+} release early in development may severely limit mitochondrial Ca^{2+} uptake and subsequent activation of mitochondrial bioenergetics. However, future experiments that directly compare mitochon-
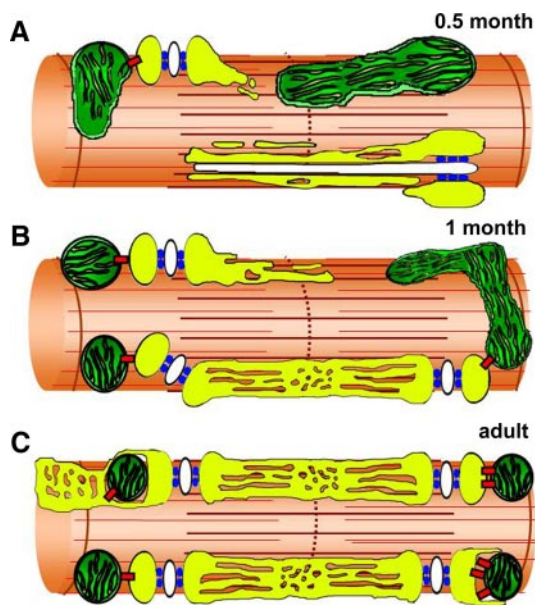

Figure 8. Model for progressive tethering of mitochondria to parajunctional positions during postnatal development. (A) At 0.5 mo after birth, mitochondria exhibit variable shapes and positioning, and the sarcotubular system is still immature. (B) Mitochondria progressively reach their parajunctional position during the first month of postnatal development. (C) In adult muscle, mitochondria are tightly tethered to CRUs between the A-I band junction and the Z-line. We propose that the primary role of tethers (red) is to trap and maintain the mitochondrion at the triad once the two organelles come in close proximity to one another during postnatal development. yellow, SR white, T-tubule; green, mitochondria; azure, RyR-feet; red, tethers.

drial Ca^{2+} uptake and mitochondrial ATP production during postnatal development will be required to more rigorously test the validity of this hypothesis.

The proposed SR mitochondrial anchoring mechanism described here for skeletal muscle is likely to be applicable to a wide variety of excitable and nonexcitable cells. Indeed, structures underlying a similar linkage have also been observed between specific ER/SR elements and mitochondria in cardiac myocytes (see Supplemental Figure S2) and liver cells (Mannella *et al.*, 1998; Csordas *et al.*, 2006). However, several unresolved questions remain to be answered. First, the molecular identity of the physical linkage between the SR and outer mitochondria membrane (i.e., tether) remains undetermined. Moreover, it will be important to determine if the tethering element is a mitochondrial protein(s), an SR protein(s), or a high-affinity interaction between complimentary proteins from both organelles. Work is also ongoing to determine if tethers solely provide a structural linkage or also exhibit direct functional activity.

ACKNOWLEDGMENTS

REFERENCES

Bagnato, P., Barone, V., Giacomello, E., Rossi, D., and Sorrentino, V. (2003). Binding of an ankyrin-1 isoform to obscurin suggests a molecular link between the sarcoplasmic reticulum and myofibrils in striated muscles. J. Cell Biol. *160*, 245–253.

Bereiter-Hahn, J., and Voth, M. (1994). Dynamics of mitochondria in living cells: shape changes, dislocations, fusion, and fission of mitochondria. Microsc. Res. Tech. *27*, 198–219.

Beutner, G., Sharma, V. K., Giovannucci, D. R., Yule, D. I., and Sheu, S. S. (2001). Identification of a ryanodine receptor in rat heart mitochondria. J. Biol. Chem. *276*, 21482–21488.

Bolanos, P., Guillen, A., Rojas, H., Boncompagni, S., and Caputo, C. (2008). The use of CalciumOrange-5N as a specific marker of mitochondrial Ca(2+) in mouse skeletal muscle fibers. Pfluegers Arch. *455*, 721–731.

Buntinas, L., Gunter, K. K., Sparagna, G. C., and Gunter, T. E. (2001). The rapid mode of calcium uptake into heart mitochondria (RaM): comparison to RaM in liver mitochondria. Biochim. Biophys. Acta *1504*, 248–261.

Crompton, M., Capano, M., and Carafoli, E. (1976). Respiration-dependent efflux of magnesium ions from heart mitochondria. Biochem. J. *154*, 735–742.

Csordas, G., Renken, C., Varnai, P., Walter, L., Weaver, D., Buttle, K. F., Balla, T., Mannella, C. A., and Hajnoczky, G. (2006). Structural and functional features and significance of the physical linkage between ER and mitochondria. J. Cell Biol. *174*, 915–921.

DiFranco, M., Neco, P., Capote, J., Meera, P., and Vergara, J. L. (2006). Quantitative evaluation of mammalian skeletal muscle as a heterologous protein expression system. Protein Expr. Purif. *47*, 281–288.

Duchen, M. R. (1999). Contributions of mitochondria to animal physiology: from homeostatic sensor to calcium signalling and cell death. J. Physiol. *516*(Pt 1), 1–17.

Duchen, M. R. (2000). Mitochondria and calcium: from cell signalling to cell death. J. Physiol. *529*(Pt 1), 57–68.

Endo, M. (2006). Calcium ion as a second messenger with special reference to excitation-contraction coupling. J. Pharmacol. Sci. *100*, 519–524.

Forbes, M. S., Plantholt, B. A., and Sperelakis, N. (1977). Cytochemical staining procedures selective for sarcotubular systems of muscle: modifications and applications. J. Ultrastruct. Res. *60*, 306–327.

Gillis, J. M. (1997). Inhibition of mitochondrial calcium uptake slows down relaxation in mitochondria-rich skeletal muscles. J. Muscle Res. Cell Motil. *18*, 473–483.

Gunter, K. K., and Gunter, T. E. (1994). Transport of calcium by mitochondria. J. Bioenerg. Biomembr. *26*, 471–485.

Ito, K., Komazaki, S., Sasamoto, K., Yoshida, M., Nishi, M., Kitamura, K., and Takeshima, H. (2001). Deficiency of triad junction and contraction in mutant skeletal muscle lacking junctophilin type 1. J. Cell Biol. *154*, 1059–1067.

Joza, N., *et al.* (2001). Essential role of the mitochondrial apoptosis-inducing factor in programmed cell death. Nature *410*, 549–554.

Koster, A. J., Grimm, R., Typke, D., Hegerl, R., Stoschek, A., Walz, J., and Baumeister, W. (1997). Perspectives of molecular and cellular electron tomography. J. Struct. Biol. *120*, 276–308.

Ladinsky, M. S., Mastronarde, D. N., McIntosh, J. R., Howell, K. E., and Staehelin, L. A. (1999). Golgi structure in three dimensions: functional insights from the normal rat kidney cell. J. Cell Biol. *144*, 1135–1149.

Lueck, J. D., Mankodi, A., Swanson, M. S., Thornton, C. A., and Dirksen, R. T. (2007). Muscle chloride channel dysfunction in two mouse models of myotonic dystrophy. J. Gen. Physiol. *129*, 79–94.

Mannella, C. A. (2006). Structure and dynamics of the mitochondrial inner membrane cristae. Biochim. Biophys. Acta *1763*, 542–548.

Mannella, C. A., Buttle, K., Rath, B. K., and Marko, M. (1998). Electron microscopic tomography of rat-liver mitochondria and their interaction with the endoplasmic reticulum. Biofactors *8*, 225–228.

Miyata, H., Silverman, H. S., Sollott, S. J., Lakatta, E. G., Stern, M. D., and Hansford, R. G. (1991). Measurement of mitochondrial free Ca^{2+} concentration in living single rat cardiac myocytes. Am. J. Physiol. *261*, H1123–H1134.

Newmeyer, D. D., and Ferguson-Miller, S. (2003). Mitochondria: releasing power for life and unleashing the machineries of death. Cell *112*, 481–490.

Nunzi, M. G., and Franzini-Armstrong, C. (1980). Trabecular network in adult skeletal muscle. J. Ultrastruct. Res. *73*, 21–26.

Ogata, T., and Yamasaki, Y. (1985). Scanning electron-microscopic studies on the three-dimensional structure of mitochondria in the mammalian red, white and intermediate muscle fibers. Cell Tissue Res. *241*, 251–256.

Ogata, T., and Yamasaki, Y. (1987). High-resolution scanning electron-microscopic studies on the three-dimensional structure of mitochondria and sarcoplasmic reticulum in the different twitch muscle fibers of the frog. Cell Tissue Res. *250*, 489–497.

Rasmussen, H., Jensen, P., Lake, W., and Goodman, D. B. (1976). Calcium ion as second messenger. Clin. Endocrinol. *5* Suppl., 11S–27S.

Rizzuto, R., Pinton, P., Carrington, W., Fay, F. S., Fogarty, K. E., Lifshitz, L. M., Tuft, R. A., and Pozzan, T. (1998). Close contacts with the endoplasmic reticulum as determinants of mitochondrial Ca^{2+} responses. Science *280*, 1763–1766.

Rizzuto, R., and Pozzan, T. (2006). Microdomains of intracellular Ca^{2+}: molecular determinants and functional consequences. Physiol. Rev. *86*, 369–408.

Rudolf, R., Mongillo, M., Magalhaes, P. J., and Pozzan, T. (2004). In vivo monitoring of Ca(2+) uptake into mitochondria of mouse skeletal muscle during contraction. J. Cell Biol. *166*, 527–536.

Scarpa, A., and Graziotti, P. (1973). Mechanisms for intracellular calcium regulation in heart. I. Stopped-flow measurements of Ca^{++} uptake by cardiac mitochondria. J. Gen. Physiol. *62*, 756–772.

Sembrowich, W. L., Quintinskie, J. J., and Li, G. (1985). Calcium uptake in mitochondria from different skeletal muscle types. J. Appl. Physiol. *59*, 137–141.

Sharma, V. K., Ramesh, V., Franzini-Armstrong, C., and Sheu, S. S. (2000). Transport of Ca^{2+} from sarcoplasmic reticulum to mitochondria in rat ventricular myocytes. J. Bioenerg. Biomembr. *32*, 97–104.

Shkryl, V. M., and Shirokova, N. (2006). Transfer and tunneling of Ca^{2+} from sarcoplasmic reticulum to mitochondria in skeletal muscle. J. Biol. Chem. *281*, 1547–1554.

Sommer, J. R., and Waugh, R. A. (1976). The ultrastructure of the mammalian cardiac muscle cell—with special emphasis on the tubular membrane systems. A review. Am. J. Pathol. *82*, 192–232.

Takekura, H., Flucher, B. E., and Franzini-Armstrong, C. (2001). Sequential docking, molecular differentiation, and positioning of T-Tubule/SR junctions in developing mouse skeletal muscle. Dev. Biol. *239*, 204–214.

Takeshima, H., Komazaki, S., Nishi, M., Iino, M., and Kangawa, K. (2000). Junctophilins: a novel family of junctional membrane complex proteins. Mol. Cell *6*, 11–22.

Territo, P. R., French, S. A., and Balaban, R. S. (2001). Simulation of cardiac work transitions, in vitro: effects of simultaneous Ca^{2+} and ATPase additions on isolated porcine heart mitochondria. Cell Calcium *30*, 19–27.